Modulation of NTC frequencies by Pc5 ULF pulsations: Experimental test of the generation mechanism and magnetoseismology of the emitting surface

S. Grimald,[1] C. Foullon,[1,2] P. M. E. Décréau,[3] G. Le Rouzic,[3] X. Suraud,[3] and X. Vallières[3]

Received 18 March 2009; revised 20 July 2009; accepted 14 August 2009; published 26 November 2009.

[1] Nonthermal continuum (NTC) radiation is believed to be emitted by the conversion of an electrostatic wave into an electromagnetic one, which takes place at the Earth's magnetic equator. It is generally accepted that the frequency of the electrostatic wave at the source meets a local characteristic frequency placed in between two multiples of the electron cyclotron frequency, f_{ce}, which results in emission of a narrow band frequency element. In an event on 14 August 2003, we compare oscillations of the central frequency of distinct NTC frequency elements observed from Cluster orbiting near perigee, with simultaneous Pc5 Ultra Low Frequency (ULF) pulsations in the magnetic field observed from the same platform. The latter magnetic perturbations are interpreted as magnetohydrodynamic poloidal waves, where fundamental and second harmonic modes coexist. The NTC oscillation and the fundamental wave have similar periods, but are phase shifted by a quarter of period. From the correlation between both signals, and the proximity of the NTC source (localized via triangulation) with Cluster, we infer that the poloidal perturbations are spatially uniform between the source and the satellites. From the phase shift between signals, we conclude that the electrostatic wave which converts into NTC is mainly governed by the plasma density, affected by movements of the magnetic field lines. Furthermore, we demonstrate that the observations can be used to perform a magnetoseismology of the emitting surface. The results show a steepening of the plasmapause density profile near the satellites, which can be responsible for the generation of NTC emission.

Citation: Grimald, S., C. Foullon, P. M. E. Décréau, G. Le Rouzic, X. Suraud, and X. Vallières (2009), Modulation of NTC frequencies by Pc5 ULF pulsations: Experimental test of the generation mechanism and magnetoseismology of the emitting surface, *J. Geophys. Res.*, *114*, A11211, doi:10.1029/2009JA014270.

1. Introduction

[2] Nonthermal continuum (NTC) radiation is, with auroral kilometric radiation (AKR), one of the two electromagnetic emissions generated within the Earth's magnetosphere and radiated into space. NTC radiation is an incoherent narrowband electromagnetic radiation of low intensity and long duration, which is observed in a frequency range from a few 100 Hz to several 100 kHz. At low frequency, below a threshold (of order 40 kHz) function of overall magnetospheric conditions, the emission appears as broadbanded, due to multiple reflections at magnetospheric boundaries. NTC radiation is observed in the Earth environment [*Gurnett*, 1975; *Etcheto et al.*, 1982; *Morgan and Gurnett*, 1991; *Kasaba et al.*, 1998; *Décréau et al.*, 2004] as well as in the environment of other magnetized planets [*Kurth*, 1992]. Terrestrial NTC emission is widely believed to be generated by conversion of electrostatic to electromagnetic waves at the plasmapause, a region of strong density gradient at the outer boundary of the plasma population corotating with the Earth. The primary electrostatic source has been suggested to be intense electrostatic waves, banded in frequency near values of the plasma frequency in the dawn outer plasmapause region and associated with 1–30 keV electrons [*Gurnett and Frank*, 1976]. The spacing between narrow spectral features has been related to the gyrofrequency at the source [*Gough*, 1982] using the relation

$$f = f_{UH} \sim (n + \delta) f_{ce}, \quad (1)$$

The NTC frequency, f, the upper hybrid frequency, f_{UH}, and the electron cyclotron frequency, f_{ce}, are defined at the source. The quantity δ, approximated to 1/2 in an earlier publication [*Kurth et al.*, 1981], can vary between 0 and 1.

[1] Mullard Space Science Laboratory, University College London, Surrey, UK.
[2] Now at Centre for Fusion, Space and Astrophysics, Department of Physics, University of Warwick, Coventry, UK.
[3] Laboratoire de Physique et Chimie de l'Environnement et de l'Espace, CNRS, Orléans, France.

0148-0227/09/2009JA014270

There is experimental evidence that NTC sources are located near the magnetic equator [*Morgan and Gurnett*, 1991], consistent with the observations of equatorial confinement of intense f_{UH} electrostatic emissions [*Gough et al.*, 1979]. At frequencies greater than the threshold quoted above (~40 kHz) NTC emission displayed the time-frequency spectrograms present narrow band elements (less than 1 kHz frequency bandwidth). Usually, the frequency bands appear as horizontal lines, although observations with 2 min period oscillatory bands have been previously reported [*Canu et al.*, 2006]. Those oscillatory bands appear quite often in the spectrograms and are correlated with oscillations in the magnetic field data.

[3] Of particular interest, for an experimental test of relation (1), is the occurrence of Ultra Low Frequency (ULF) hydromagnetic oscillatory perturbations in the dipolar magnetic field [e.g., *Anderson*, 1994]. Such magnetic perturbations can modulate ion cyclotron frequencies [e.g., *Loto'Aniu et al.*, 2009]. At the same time, they are expected to modulate the local electron cyclotron frequency and, by way of equation (1), the NTC frequency. In this paper, we present an event observed at a Cluster perigee pass, at both sides of the magnetic equator, where oscillatory frequency bands are identified in the spectrograms of the four Cluster spacecraft. These oscillations show the same period as Pc5 pulsations observed in the magnetic field data. The large oscillatory period allow us to estimate the source position and to compare the wave observations with the magnetic field ones. Section 2 presents the plasma wave and magnetic field observations. Section 3 discusses the frequency pattern and source positioning. Section 4 discusses an experimental test of equation (1) and develops a magnetoseismology of the emitting surface. Conclusions are given in Section 5.

2. Observations

2.1. Cluster Constellation and Waves of High Frequency and Sounder for Probing of Electron Density by Relaxation Data

[4] The Cluster mission consists of four identical satellites (denoted C1, C2, C3 and C4) in a tetrahedral configuration. They travel in a near-polar orbit with perigee located at ~4.5 R_E near the ecliptic. On 14 August 2003, the constellation travels in the dipolar region for a couple of hours near perigee. During the observation, interspacecraft separation distances are less than 0.25 R_E. The four Cluster satellites crossed the magnetic equator between 11:10 UT and 11:25 UT at about 13:15 MLT.

[5] Observations presented in this paper are derived mainly from the Waves of High frequency and Sounder for Probing of Electron density by Relaxation (WHISPER) instruments. Each WHISPER instrument is a relaxation sounder [*Décréau et al.*, 1997, 2001] using for reception one of the two long double sphere antennas of the Electric Field and Wave (EFW) instrument [*Gustafsson et al.*, 1997]. The receiving antenna has a sphere-to-sphere separation of 88 m and rotates in the spin plane, which is parallel to the $X_{GSE} - Y_{GSE}$ plane (where GSE refers to geocentric solar ecliptic system), at a 4 s period. The wave form is acquired and a FFT (Fast Fourier Transform) performed every 13.33 ms. Accumulated frequency spectra are delivered every 2 s [*Décréau et al.*, 2001]. Sounding operations provide the electronic plasma frequency (f_{pe}) and the electronic cyclotron frequency (f_{ce}) at a recurrence of 52 s or 104 s. Spectral signatures on natural emissions offer a better resolution.

[6] Figure 1 presents data from the WHISPER instrument on board C4. The vertical dot-dashed line indicates the magnetic equator crossing. The satellite comes from the Southern hemisphere and travels to the Northern hemisphere indicated respectively by SH and NH in Figure 1a. Figure 1a presents a time-frequency spectrogram of electric field measured by WHISPER in its passive mode on board C4. The time interval shown, 10:40–11:40 UT, includes the phenomenon of interest, i.e., NTC emissions, present on both sides of the equator, at frequencies above the plasma frequency, f_{pe}, indicated by a solid white line. The f_{pe} increases and decreases during the observation time range, spanning a range of frequencies between 35 and 53 kHz, indicating a plasmapause crossing. However, the smooth variation of the plasma frequency shows that the spacecraft only intercept the outer plasmasphere, as the main plasmasphere body appears to have been compressed to L values below Cluster orbits. At about 11:15 UT, C4 crossed the magnetic equator, where localized intense electrostatic emissions are seen at frequencies $(n + 1/2)\, f_{ce}$ lying below f_{pe}. Such emissions, first observed on board OGO 5 [*Kennel et al.*, 1970], coexist in this event with intense equatorial emissions above f_{pe} at ~63 kHz, close to the Bernstein frequencies f_{qs} [*Bernstein*, 1958], identified by the sounder in active mode. The latter emissions could be primary (electrostatic) source of NTC, invoked in the nonlinear decay generation mechanism proposed by *Rönnmark* [1985]. In addition, intense emissions are observed on each side of the magnetic equator at ~55 kHz: they seem to be intensifications of a signal at f_{UH} (just above the plasma frequency) and are other candidates for primary sources of NTC.

[7] Figure 1b shows in greater details the NTC emissions. They are observed continuously from the southern hemisphere to the northern hemisphere with different spectral signatures. In the northern hemisphere, the emission intensity is quasi-homogeneous in a 60 to 80 kHz frequency range. In the southern hemisphere, and for the same frequency range, some narrow frequency bands (less than 1 kHz frequency width) are more intense than the average level. Note also in the southern hemisphere, near 50 kHz, emissions at frequency f_q, shown inside a rectangular box in Figure 1b. The frequency position of the peak emission observed in this band varies quasi periodically with time, mimicking the time variation of the local plasma frequency.

[8] In order to better visualize the frequency pattern of NTC emissions, the spectrogram has been treated as follow: each frequency spectrum has been normalized to the dynamical range covered by the spectrum (after this treatment, all spectra present intensities varying between the same two levels, minimum and maximum). Then, in each spectrum, all intensity maxima (frequency peaks) have been identified, and only those placed above a chosen intensity level have been selected. The result is displayed in Figure 1c. In the northern hemisphere, this treatment highlights series of quasi-monochromatic emissions (horizontal lines) of few minutes duration, showing up above the local plasma frequency (black curve). Hence, the continuous form appearing in the northern hemisphere (right side) of Figure 1b, can

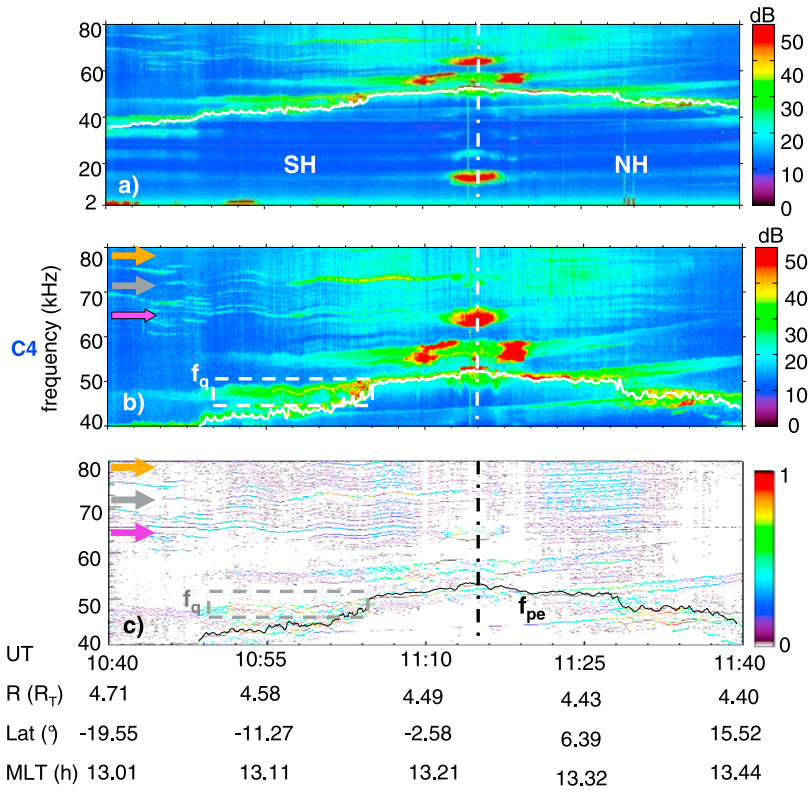

Figure 1. Frequency-time spectrograms of natural emissions observed on 14 August 2003 by the WHISPER instrument on board C4. Spectrograms of wave intensity reported in dB above 10^{-7} V_{rms} $Hz^{-1/2}$ (a) in the 2–80 kHz frequency range and (b) centered on NTC radiation. (c) Positions of intensity maxima in the 40–80 kHz frequency range (lower maxima are suppressed, see text). In Figures 1b and 1c, three horizontal arrows indicate NTC frequency bands at 65 kHz (violet), 72 kHz (gray), and 79.5 kHz (orange). Vertical dot-dashed lines (white in Figures 1a and 1b and black in Figure 1c) indicate the position of the plasma frequency f_{pe}. The form framed with a dashed line contour underlines the frequency band marked with a peak at Bernstein frequency f_q.

be sorted in frequency elements, each of them with its own maximum of intensity. Those elements are so close in frequency to each other (the frequency separation not far above the instrumental resolution) and their intensities so similar that they are difficult to distinguish in the original spectrogram. In the southern hemisphere the frequency pattern, highlighted by the treatment (left side of Figure 1c), shows oscillatory frequency elements. The period of oscillation, P_0, of each element depends slightly of its average frequency, f_0. Three elements are indicated by a violet (f_0 = 65 kHz), a gray (f_0 = 72 kHz) and an orange arrow (f_0 = 79.5 kHz). In order to visualize the link between P_0 and f_0, Figure 2 presents the evolution of $\Delta f = f - f_0$, where f is the measured frequency of a given band. The color code refers to the three different elements. Figure 2 shows that P_0 increases when f_0 decreases and that the instantaneous phase of the three oscillatory signals Δf is the same near the center of the time interval (at 11:03 UT). The three frequency bands at mean frequency f_0 of 65, 72 and 79.5 kHz are modulated with periods P_0 of 7 min 10 s, 6 min 30 s and 5 min 27 s respectively. We note also that the emission at frequency f_q near 50 kHz is modulated with a period about twice smaller.

2.2. Pc5 Pulsations

[9] Figure 3 presents measurements from the Fluxgate Magnetometer (FGM) instruments [*Balogh et al.*, 2001] on board the 4 spacecraft in the SM (Solar Magnetic) coordinates, when the satellites are in the Southern hemisphere. The three components and the amplitude of the magnetic field are represented in Figures 3a–3d and the color codes refer to the various satellites (black is C1, red is C2, green is C3, blue is C4). ULF Pc5 pulsations are observed in the data. These oscillations appear in phase between the four spacecraft which are located at L shells ranging between 4.68 R_E to 4.76 R_E. ULF waves in the Pc5 frequency range (1–10 mHz) usually appear on the duskside magnetosphere under storm or substorm conditions [*Hudson et al.*, 2004]. The event under study occurs during a very disturbed period. As observed in the Dst index, two moderate storms (-50 nT $\leq$ Dst ≤ -100 nT [see *Loewe and Prölss*, 1997]) occur on 6 and 8 August 2003, followed by a long recovery phase punctuating with numerous weak storms. Within this recovery phase period, at the time of observation, on 14 August, the Kp index is low (Kp = 2), which normally indicates the plasmapause to be far from Earth (see *Pierrard and Lemaire* [2004] for a link between the plasmapause position and the Kp index). However, the earlier active geomagnetic conditions have affected the plasmapause, such that it has been likely compressed to low L values and that its position, below Cluster perigee, cannot be evaluated accurately. In this case event a new plasmapause knee, in formation, is observed at L $\sim$ 10 (not shown).

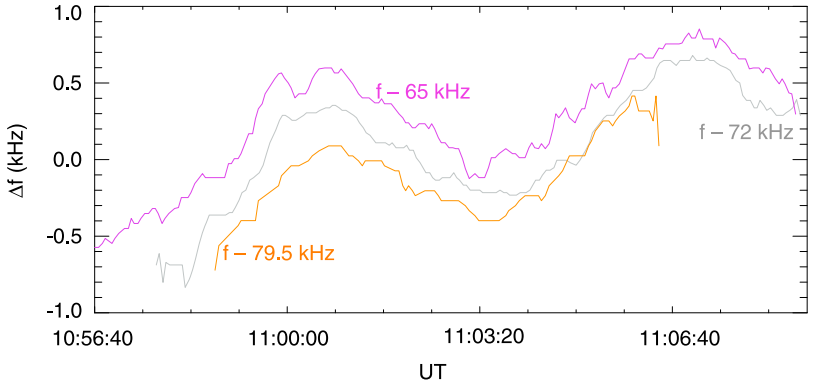

Figure 2. Frequency evolution with time of three NTC bands with respect to their average frequency f_0, showing $\Delta f = f - f_0$, where f is the measured frequency of a band at an average frequency f_0 of 65 kHz (violet), 72 kHz (gray), or 79.5 kHz (orange).

[10] Pc5 pulsations are observed in the magnetic field components, and dominate in Bx, shown in Figure 3a and Bz, shown in Figure 3c. Figure 3e shows the magnetic field deviations at C4 from a magnetospheric model [*Tsyganenko*, 1989] in the SM system, viz. $\Delta B = B - B_{model}$. Aspects of the pulsations for this particular event have been previously studied by *Eriksson et al.* [2005], who use a field-aligned coordinate system. In this field-aligned coordinate system, the magnetic field exhibits the poloidal mode polarization of a magnetohydrodynamic (MHD) wave, with perturbations mainly in the radial and field-aligned components. The azimuthal, m, wave number is thought to be large. The spacecraft are too close to each other to make a precise determination of this m number [*Eriksson et al.*, 2005]. However, perturbations in ΔBy indicate a mixed (toroidal/poloidal) polarity. The Pc5 pulsations are seen in the southern hemisphere and damp near the magnetic equator crossing (at the closest approach to the inner plasmapause). The dominant frequency is about 5.8 mHz (period 2 min 52 s) when the spacecraft are south of the magnetic equator. Close to the magnetic equator and the inner plasmapause (∼11:15 UT), the amplitudes of the magnetic perturbations decrease and disappear. This behavior is similar to the NTC frequency oscillatory behavior. As the spacecraft move north of the equator, the large perturbations in the magnetic field reappear and oscillate at a dominant frequency of 5.4 mHz or period of 3 min 05 s (not shown [see *Eriksson et al.*, 2005]).

[11] Figure 3f shows the Pc5 oscillations in the velocity field (in SM coordinates) measured by EFW on C4. The 3 min pulsations dominate in the components Vx and Vz. For these 3 min pulsations, Figures 3e and 3f show that the perturbations ΔBx lag the velocity perturbations in Vx (corresponding to electric field oscillations Ey) by a quarter of period. Together with the absence of waves near the magnetic equator, this is a signature of a second harmonic oscillation [e.g., *Singer et al.*, 1982; *Takahashi and Anderson*, 1992; *Schäfer et al.*, 2008]. By 10:48 UT, we see in Figure 3e the appearance of larger magnetic perturbations, mostly in ΔBx, with periodicities (6 min 36 s), about twice as long as the ones found previously. In the velocity field, Vx remains unaffected, with oscillations around 3 min. The 3 min oscillations can also be found in ΔBx after high-pass filtering. The longer periodicities are akin to a fundamental. Poloidal waves are usually observed in the second rather than the fundamental harmonic [e.g., *Takahashi and Anderson*, 1992]. This is supported by theoretical studies [*Cheng and Lin*, 1987]. However, *Mager and Klimushkin* [2006] predict the fundamental to be observed and argue that its absolute amplitude is considerably larger than those of the harmonics. For a fundamental poloidal mode, the largest amplitude in ΔBx at the equator is expected to correspond to a node in perturbations of Bz, Vx and density, ρ. For the second harmonic, the largest perturbations in the latter variables would correspond to a node in ΔBx at the equator. This is qualitatively consistent with the measurements, which are taken relatively close to the equator. Therefore, the Pc5 magnetic pulsations are interpreted as MHD poloidal waves, where fundamental and second harmonic modes coexist.

3. Study of the NTC Bands in the Southern Hemisphere

3.1. Stability of the Sources

[12] We focus now on the behavior of NTC frequency elements observed in the southern hemisphere, between 10:40 UT and 11:08 UT by C4 (Figure 1), and at similar time intervals by the other spacecraft. Near perigee, the Cluster tetrahedron is elongated (Figure 4b). The interspacecraft separation distance ranges from ∼300 km (C2 and C3) to 1100 km (C1–C4). C1 is leading, and then come C3, C2, and C4 brings up the rear. In Figure 4, color codes refer to the various satellites (black is C1, red is C2, green is C3, blue is C4). Figure 4a presents the frequency evolution versus time of the intensity peaks observed by the four Cluster spacecraft in the band 71–74 kHz (indicated for C4 by the gray arrow in Figures 1b and 1c). The gray surface covers the frequency bandwidth of the NTC element observed by C1. The plot indicates that the four satellites observe simultaneously the same frequency versus time evolution of the NTC element, despite their different positions.

[13] In order to compare signal amplitudes between spacecraft, we show the electric field amplitude between 10:56 UT and 11:10 UT versus time in Figure 4b and versus magnetic latitude, in Figure 4c, for a given frequency, 72 kHz, indicated in Figure 4a by a horizontal dashed line. The constellation along the orbit at 11:00 UT is in a line of pearls configuration, as shown on the left of Figure 4b.

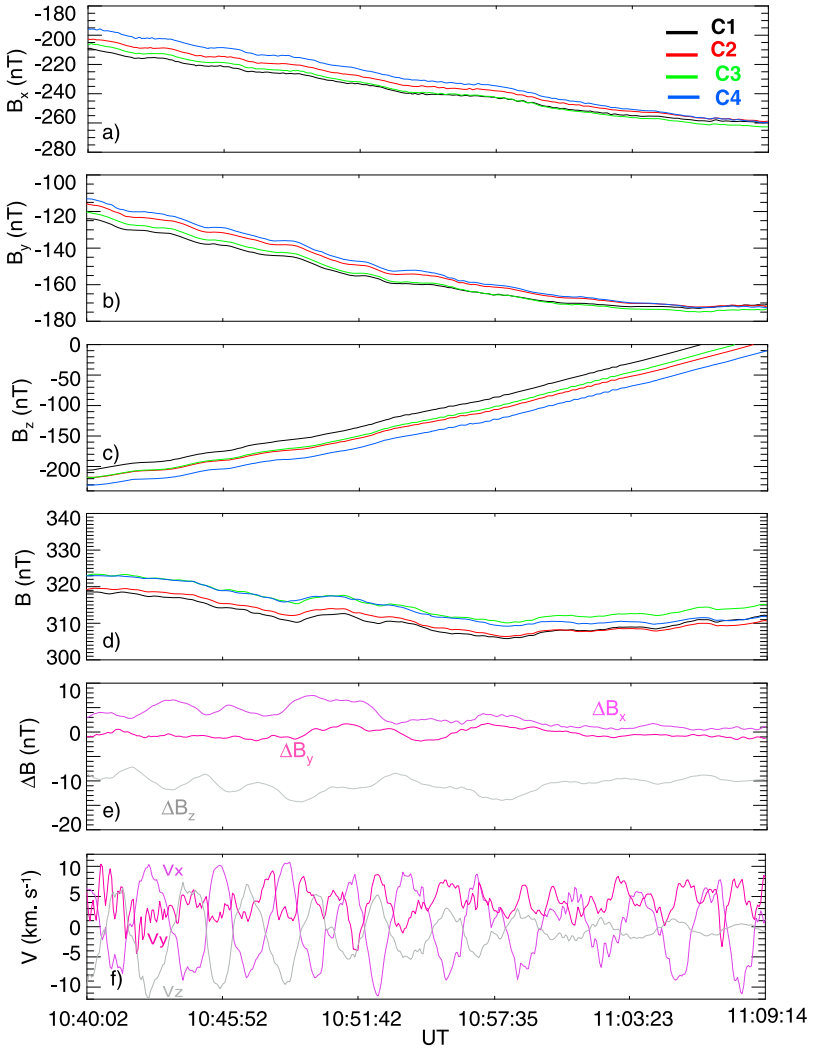

Figure 3. Magnetic field and velocity field measurements shown in the SM coordinate system when oscillatory NTC band emissions are detected in the Southern Hemisphere: multispacecraft observations of (a–c) magnetic field components and (d) magnitude (C1 is black, C2 is red, C3 is green, C4 is blue) and observations at C4 of (e) magnetic field component variations from a background magnetospheric model and (f) velocity field components.

According to Figure 4a, where the dashed line intercepts the band twice, the time evolution of the electric field amplitude indicates two consecutive increases of intensity. This evolution is observed by the four satellites, with maximum observed at 10:58:10 UT and 11:03:31 UT, and indicated respectively by orange and violet arrows in Figure 4. The second intensity increase and the corresponding peak are observed simultaneously by the four satellites (peaking at 11:03:31 UT) and at different magnetic latitudes, which are ordered exactly in the line of pearls configuration of the satellites (Figure 4c). This suggests a scenario where a single source emits a beam large enough to illuminate the four satellites simultaneously, during the whole observation between 10:56:40 UT and 11:10 UT. Therefore we deduce that the observed NTC element, modulated in frequency, stems from the same emitting source. Contrary to the second peak (peaking at 11:03:31 UT), the first intensity increase is not observed to start and peak at the same time by the four Cluster satellites (Figure 4b). This observation can be analyzed in more details taking into account the limited size of the cone angle, but this study is beyond the scope of this paper. It is also useful to note here that an analysis of the observations for each of the other measured frequency bands yields the same results.

3.2. Position and Movement of the Source

[14] Assuming that this NTC radiation is electromagnetic and propagating in the O mode (quasi-circular polarization), the spin modulation can be used to determine the projection of the direction of propagation onto the antenna spin plane [*Calvert*, 1985; *Gurnett*, 1975; *Gough*, 1982; *Kasaba et al.*, 1998; *Décréau et al.*, 2004]. The modulation index factor (ratio of modulated signal to total power over several spin periods), mi, and the ak angle (angle between X_{GSE} axis and raypath direction, projected onto the $X_{GSE} - Y_{GSE}$ plane are derived from this process. The mi and the ak values calculated between 10:56:28 UT and 11:13:43 UT in a 40–80 kHz frequency range are presented respectively in

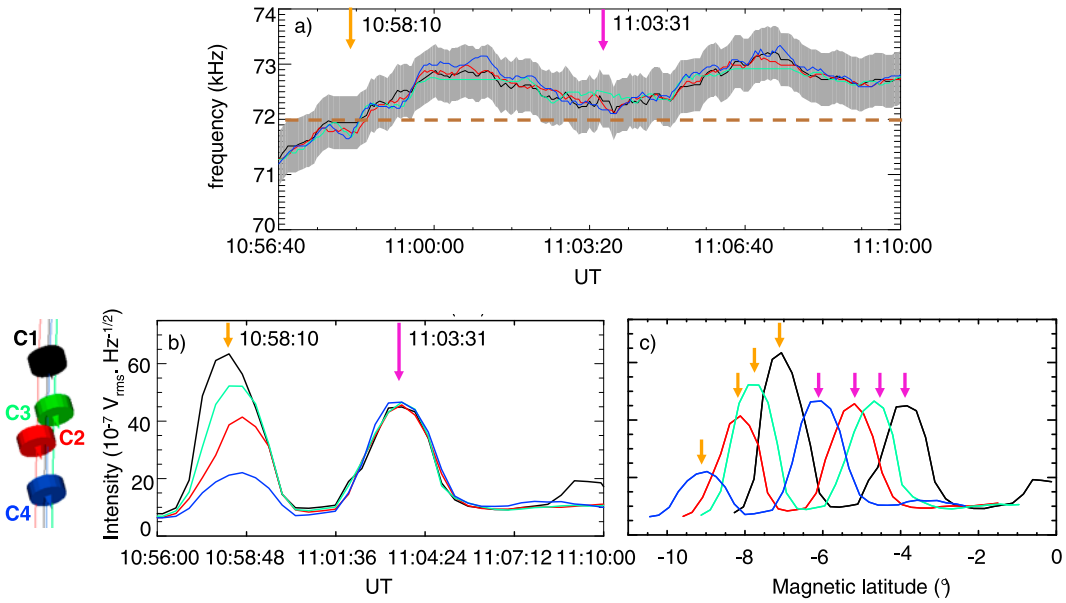

Figure 4. Multispacecraft observations of one NTC band by C1 (black), C2 (red), C3 (green), and C4 (blue) showing (a) a frequency evolution with time of the NTC band observed between 71 and 74 kHz and (b) temporal and (c) latitudinal profiles of electric field amplitude measured by each of the four satellites at 72 kHz. Latitudes are expressed in SM coordinates. The spacecraft configuration at 11:00 UT is shown on the left of Figure 4b. This multispacecraft study suggests that a single source illuminates the four spacecraft at the same time, the frequency of the source changing during the observations.

Figures 5a and 5b. The ak angle displays a gradual evolution along the orbit, with a value about constant in all the frequency range at a given time. Therefore, the sources producing the series of narrow band elements observed in the quoted frequency range are all projected in a same source region of small extension around which the satellites travel. As in Figure 1, the band around 72 kHz is pinpointed by a gray arrow. The mi values for the corresponding frequencies are between 70% and 100%. In the 10:59 to 11:13 UT interval, covering roughly two oscillations of the NTC frequency peak, the band displays modulation index values higher than 90%, indicating a source located close from the spin plane during the time interval. We interpret the small increase and decrease of mi as a movement of small amplitude, along the Z_{GSE} axis, of the source with respect to the satellite.

[15] When the source is punctual and stable with time, the projections onto the spin plane of the various raypaths can be used to estimate source positions by triangulation using raypaths at different times [*Morgan and Gurnett*, 1991]. Only a 2D picture of directivity in the $X_{GSE} - Y_{GSE}$ plane can be achieved from such measurements by Cluster. Figure 6 displays the orbits of the four Cluster satellites projected into this plane as well as the directivity paths plotted between 10:56:40 UT and 11:10 UT. It is remarkable that all the lines cross in the same region, thus pointing to a source region stable in this plane during the total time interval considered. This source region, indicated by the gray star, is small, about 0.06 R_E in diameter. It is located at about 4.23 R_E from the Z_{GSE} axis and 0.3 R_E from Cluster orbit. The relative distance from satellite to source could vary along the Z_{GSE} direction, up to an amount corresponding to the amplitude of mi values variations. However, noting that the mi (modulation index) measurement carries a large uncertainty factor, and that the distance traveled by the satellite along Z_{GSE} is significant (of the same order of magnitude than the source to spacecraft distance in the XY plane), it is difficult to estimate what is the source movement proper. In any event, the mi value measured (~90%) fits the assumption of a source lying in the magnetic equatorial plane, where the XY GSE and XY SM planes are about 0.2 RE apart at the geocentric distance of the NTC source.

4. Discussion

4.1. Modulation of NTC Frequencies by ULF Pc5 Pulsations

[16] We investigate whether the link between the two oscillatory phenomena can be further explained and whether this may shed light on the generation mechanism of the NTC emission. We pose that: (i) the frequency of NTC emissions are modulated by the Pc5 pulsations which are interpreted in terms of a spatially localized (fundamental poloidal) MHD wave, (ii) the region bounded between the NTC source position, estimated by triangulation, and the outermost Cluster position during the time interval when modulated NTC elements are observed, can be considered as undergoing stationary oscillations. To study in more details the link between NTC bands and magnetic field lines oscillations, we compare the oscillations observed in situ in the magnetic field amplitude and in the magnetic field components with those observed in the NTC bands. In Figure 7, the oscillations in the magnetic field are highlighted, as in Figure 3e, by subtracting a background field [*Tsyganenko*, 1989] from the measured magnetic field, but the time series are presented this time in cylindrical coordinates (R_{XY} in the equatorial plane, Z parallel to the Z_{SM}

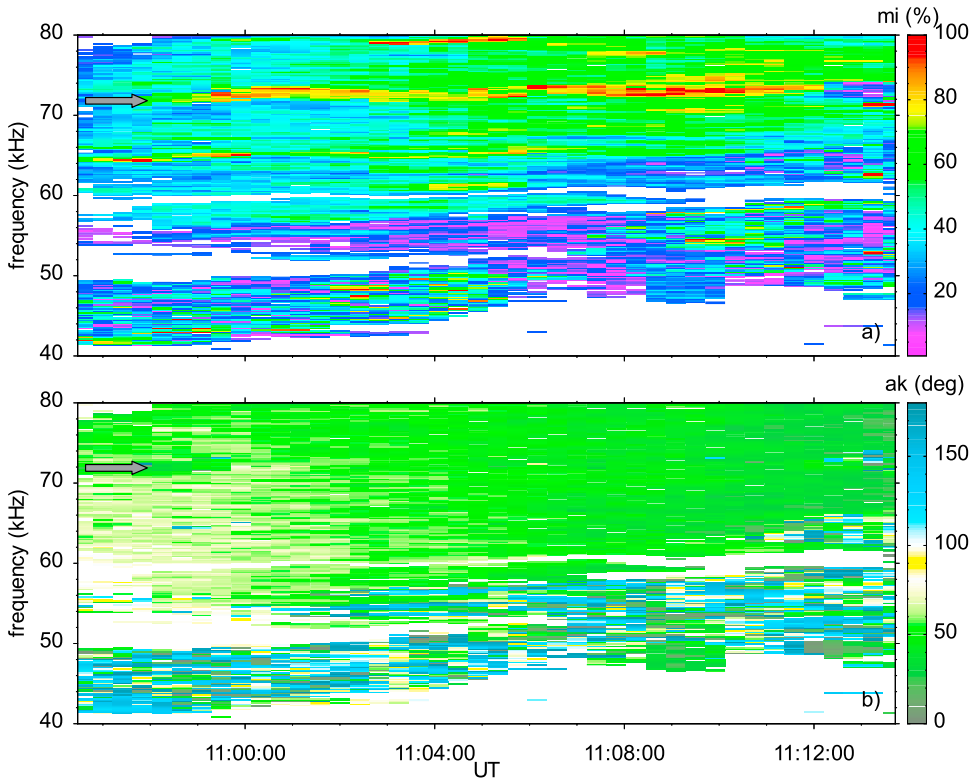

Figure 5. Parameters derived from spin modulation of electric field intensity, plotted as frequency-time spectrograms of (a) modulation index m and (b) directivity angle ak. The gray arrows point to the NTC band at ~72 kHz.

axis). As shown in Figure 7, B_{rxy} (in violet) and B_z (in gray) oscillate with different dominant periods, the B_{rxy} oscillation period being about twice the B_z period, which correspond to the fundamental and harmonic oscillations respectively. The oscillations observed in the magnetic field amplitude (in orange) follow those from B_z. For comparison the NTC frequency band observed at f_0 = 72 kHz is added (in black) in the top of Figure 7.

[17] First, we note that the NTC band oscillations reflect only the oscillations in the B_{rxy} component, at fundamental frequency, in accordance with the assumption of a (remote) NTC source lying close to magnetic equator. The source, which is either fixed in space, or moves in the Z_{GSE} direction, but remaining close to the magnetic equatorial plane, is not affected by oscillations in B_z and the magnetic field amplitude (at second harmonic). Second, we note that the NTC band oscillations and the oscillations in the B_{rxy} component are phase shifted by a quarter of period (like sine and cosine functions, see Figure 8a). To confirm and characterize the phase shift, we perform the cross correlation between the time series as shown versus time lags in Figure 8b. The coefficients reach a statistically significant peak (above 0.8) indicating a good correlation and a phase shift of about 1.6 min.

[18] From equation (1), a small variation of the frequency f of NTC oscillations can be due either to a small variation of the n_{th} harmonic of the electron gyrofrequency, f_{ce}, or to a small variation of the parameter δ. We think that the latter parameter is directly linked to the f_p/f_{ce} ratio, like in the case where the characteristic frequency f would be linked to the Bernstein frequency f_{qn} attached to the harmonic band concerned. Therefore, NTC elements oscillations may be linked with plasma density oscillations phase shifted with the magnetic field equatorial component by a quarter of period. This is typically expected for the compressional mode associated with the poloidal mode. This mode is generally a fast MHD mode, for which, contrary to the slow MHD mode, the longitudinal flow, Vz, does not dominate over the other components. This signature is confirmed with EFW data of plasma velocities (Figure 3f).

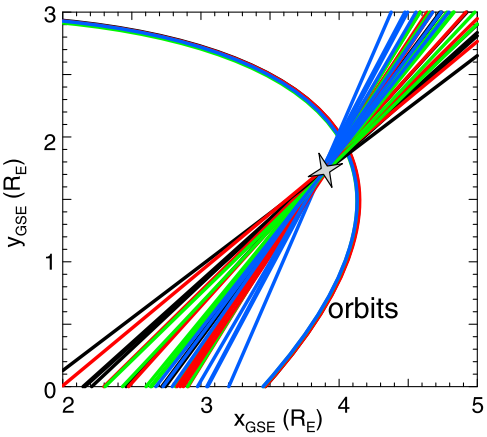

Figure 6. Triangulation in the XY GSE plane for the band observed between 71 kHz and 74 kHz. Directivity lines drawn from each satellite (C1 is black, C2 is red, C3 is green, C4 is blue) indicate a source (gray star) stable over the total time interval.

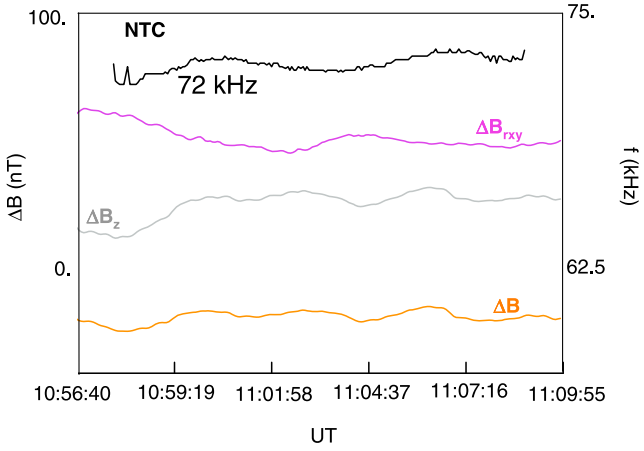

Figure 7. Qualitative amplitude variations of magnetic field component in spherical coordinates (violet, gray, and orange). For comparison, the peak frequency (arbitrary units) of NTC element observed at $f_0 \sim 72$ kHz is added (black curves) in the top and bottom.

Note finally that the second harmonic appears to modulate f_q (as well as the local plasma frequency). A comparison (not shown) of those modulations on the different Cluster spacecraft indicates that crossings of a phase reference (positions of a minimum in frequency) are organized in time according to the relative positions of the spacecraft (first encounter by C1, then by C3, C2, and C4, respectively), which supports our assumption of a homogenous region undergoing stationary oscillations.

4.2. Magnetoseismology of the Emitting Surface

[19] From the propagation direction analysis in Section 3, we infer that each of the three sources of the emissions pinpointed by the orange, gray and violet arrows in Figure 1 are modulated by the same uniform density disturbances spatially localized in the L shell direction at the plasmapause. As discussed above (Section 4.1), such disturbances are likely to be caused by the poloidal (fundamental) fast mode of an MHD wave with wavelength function of the L shell radius, L, at the source position. The NTC sources are localized in the plasmapause density gradient, in a region where f_{UH} is approximately the electron plasma frequency, f_{pe}. We now demonstrate that the observations of series of NTC frequency bands modulated by the MHD wave can be used to determine the spatial locations on radial L shells of their respective sources. In other words, we perform a magnetoseismology of the emitting surface. Our aims are twofold. First we wish to confirm that the wave is spatially localized on a radial L shell distance consistent with the typical widths of $1-2$ R_E found by other experiments [*Hughes et al.*, 1977; *Singer et al.*, 1982; *Engebretson et al.*, 1992]. Second, we wish to visualize the frequency or density profile of the plasmapause, which is responsible for the generation of NTC emission. We proceed as follows.

[20] The period of the fast poloidal MHD wave is approximately $P \sim a\ L/V_A$, where V_A is the local Alfven speed at the source position and a is a factor due to the field line length and increasing with L [e.g., *Mann and Wright*, 1995]. Due to the dependence of V_A and f_{pe} on the plasma density, the periods $P_0 = P$ and mean frequency f_0 of the NTC emission are expected to correlate as follows: $P_0/f_0 \sim b(L)\ L/B_0$, where $b(L)$ is a value expected to increase with L, and B_0 is the magnetic field at the source position, which can be further approximated as a dipole field $B_0 \sim M\ L^{-3}$ for dipole moment M [see also *Denton et al.*, 2003]. Therefore, we finally obtain the relation

$$P_0/f_0 = \alpha^2(L)L^4, \tag{2}$$

with value α in s. R_E^{-2} and expected to increase with L. Applying this relation for each of the NTC emitting band and assuming a range of values α for the L shells of interest, it may be possible to give, within error bars, the shape of the emitting surface.

[21] Since α is expected to be a slowly increasing function of L for the region of interest, we determine the range of values α from a linear approximation between two values, to be calculated respectively (a) at the position known by triangulation of the source of the middle band (emitted at $f_0 = 72$ kHz) and (b) at the spacecraft position.

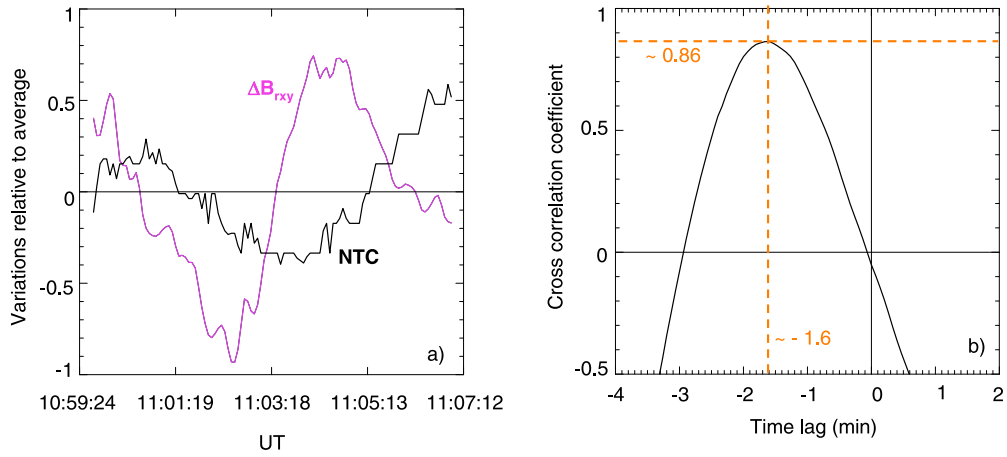

Figure 8. (a) Variation time series (relative to average) of the equatorial magnetic field component (in nT) and the NTC peak frequency at $f_0 \sim 72$ kHz (in kHz) and (b) their corresponding cross-correlation coefficients versus lag times.

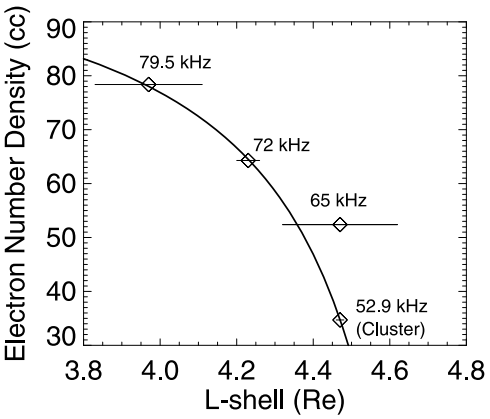

Figure 9. Electron number density profile of the plasmapause versus radial L shell near the Cluster spacecraft. A hyperpolic curve is fitted to estimates with error bars derived from a magnetoseismology of the NTC radiation-emitting surface and including a measurement at the Cluster location (most outward from the Earth). The profile shows a steepening of the plasmapause density near the satellites, which can be responsible for the generation of NTC emission.

The two calculated values of α^2 are 1.692×10^{-5} and 1.875×10^{-5} s^2. R_E^{-4}, at respective L shells of 4.23 and 4.47 R_E, plasma frequencies f_0 of 72 and 52.9 kHz and modulation periods P_0 of 390 s (6 min 30 s) and 396 s (6 min 36 s). This confirms that α is an increasing function of L. Thus, for the region of interest, a simple linear approximation between the two values yields

$$\alpha^2(\mathrm{L}) = (-1.5361 + 0.7631\ \mathrm{L}) \times 10^{-5} \mathrm{s}^2.\ \mathrm{R_E}^{-4}. \qquad (3)$$

We then deduce an average value at the plasmapause for a range of L shells centered at L = 4.2 ± 0.3 R_E, viz. $\alpha^2 = (1.67 \pm 0.23) \times 10^{-5}$ s^2. R_E^{-4} and apply equation (2) for the source positions of the other bands. We obtain L shells L = 4.47 ± 0.15 R_E and L = 3.97 ± 0.14 R_E at frequencies of 65 kHz and 79.5 kHz respectively.

[22] As a result, Figure 9 presents a density profile of the plasmapause, where the density corresponding to the plasma frequency is shown at each of the four known or inferred L shells (for each of the three bands and at the Cluster location). Thus we confirm that the wave is spatially localized on a radial L shell distance of at most 0.5 RE, well within the typical widths of 1–2 R_E found by previous experiments. Moreover, the profile shows a steepening of the plasmapause density near the satellites, which can be responsible for the generation of NTC emission.

5. Summary and Conclusion

[23] In this paper, we have analyzed an event on 14 August 2003, observed at the Cluster perigee pass, at about 13 MLT. In this event, oscillations are observed in a series of NTC frequency bands with similar periods than ULF Pc5 pulsations, detected simultaneously in the magnetic field data. The latter magnetic perturbations are interpreted as MHD poloidal waves, where fundamental and second harmonic modes coexist. The NTC oscillation period is similar to the period of the fundamental mode. The data analysis on the available data sets provides here the NTC source localization, a discussion of the mechanism of generation of NTC radiation and a study of the shape of the emitting surface. It has been shown that the NTC emission in all frequency bands comes from a small source region located not far from the satellites' orbits when the spacecraft cross the magnetic equator. These observations allow a quantitative test of equation (1), by comparing the NTC frequency oscillations with Ultra Low Frequency (ULF) Pc5 oscillations in the magnetic field, which are expected to modulate f_{ce}. However, the two oscillations are phase shifted by a quarter of period. From the localization of the NTC source at 0.3 R_E Earthward from Cluster, we assume that the poloidal perturbations are spatially uniform between the source and the satellites. From the nature of phase shift between both oscillations, we infer that the electrostatic wave, which converts into NTC, is mainly driven by the plasma density modulation. Some mechanisms implying the Bernstein modes were developed by *Rönnmark* [1985], *Melrose* [1981], *Christiansen et al.* [1984], and *Oya* [1971]. Those mechanisms seem to be more relevant here but remain to be tested. Furthermore, we demonstrate that the observations of series of NTC frequency bands modulated by Pc5 pulsations, interpreted in terms of a spatially localized MHD wave, can be used to perform a magnetoseismology of the emitting surface. The results show a steepening of the plasmapause density profile near the satellites, which can be responsible for the generation of NTC emission. Since ULF pulsations occur relatively often in the magnetosphere [see, e.g., *Anderson*, 1994] for occurrence and spatial distributions), the emission mechanisms for NTC radiation can be further tested and the emitting surface of the plasmapause can be better studied with more observations and experiments.

[24] **Acknowledgments.** S.G. and C.F. acknowledges financial support from the UK Science and Technology Facilities Council (STFC) on the MSSL rolling grant. We would like to thank the WEC, JSOC, and ESOC teams for continuous support of Cluster operations. S.G. and C.F. thank P. Décréau, J. G. Trotignon, and the WHISPER team; E. Lucek and the FGM team; and M. André and the EFW team for preparing the data used in this paper and the CAA for providing it. The authors also would like to thanks the QSAS team for providing the QSAS software.

[25] Zuyin Pu thanks Viviane Pierrard for her assistance in evaluating this manuscript.

References

Anderson, B. J. (1994), An overview of spacecraft observations of 10 s to 600 s period magnetic pulsations in the Earth's magnetosphere, in *Solar Wind Sources of Magnetospheric Ultra-Low-Frequency Waves*, *Geophys. Monogr. Ser.*, vol. 81, edited by M. J. Engebretson et al., pp. 25–43, AGU, Washington, D. C.

Balogh, A., et al. (2001), The Cluster magnetic field investigation: Overview of in-flight performance and initial results, *Ann. Geophys.*, *19*, 1207–1217.

Bernstein, I. B. (1958), Waves in a plasma in a magnetic field, *Phys. Rev.*, *109*, 10–21, doi:10.1103/PhysRev.109.10.

Calvert, W. (1985), DE-1 measurements of AKR wave directions, *Geophys. Res. Lett.*, *12*, 381–384, doi:10.1029/GL012i006p00381.

Canu, P., P. Décréau, S. Escoffier, and S. Grimald (2006), Observations of continuum radiations close to the plasmapause: Evidence for small scale sources, in *Planetary Radio Emissions VI*, edited by H. O. Rucker, W. S. Kurth, and G. Mann, pp. 289–297, Austrian Acad. of Sci., Vienna.

Cheng, C. Z., and C. S. Lin (1987), Eigenmode analysis of compressional waves in the magnetosphere, *Geophys. Res. Lett.*, *14*, 884–887, doi:10.1029/GL014i008p00884.

Christiansen, P. J., J. Etcheto, K. Rönnmark, and L. Stenflo (1984), Upper hybrid turbulence as a source of nonthermal continuum radiation, *Geophys. Res. Lett.*, *11*(2), 139–142, doi:10.1029/GL011i002p00139.

Décréau, P. M. E., P. Fergeau, V. Krasnoselskikh, M. Lévêque, P. Martin, O. Randriamboarison, F. X. Sené, J. G. Trotignon, P. Canu, and P. B. Mögensen (1997), WHISPER, a resonance sounder and wave analyser: Performances and perspectives for the Cluster mission, *Space Sci. Rev.*, *79*, 157–193, doi:10.1023/A:1004931326404.

Décréau, P. M. E., et al. (2001), Early results from Whisper instrument on Cluster: An overview, *Ann. Geophys.*, *19*, 1241–1258.

Décréau, P. M. E., et al. (2004), Observation of Continuum radiations from the Cluster fleet: First results from direction finding, *Ann. Geophys.*, *22*, 2607–2624.

Denton, R. E., M. R. Lessard, and L. M. Kistler (2003), Radial localization of magnetospheric guided poloidal Pc 4-5 waves, *J. Geophys. Res.*, *108*(A3), 1105, doi:10.1029/2002JA009679.

Engebretson, M. J., D. L. Murr, K. N. Erickson, R. J. Strangeway, D. M. Klumpar, S. A. Fuselier, L. J. Zanetti, and T. A. Potemra (1992), The spatial extent of radial magnetic pulsation events observed in the dayside near synchronous orbit, *J. Geophys. Res.*, *97*, 13,741–13,758, doi:10.1029/92JA00992.

Eriksson, P. T. I., L. G. Blomberg, A. D. M. Walker, and K.-H. Glassmeier (2005), Poloidal ULF oscillations in the dayside magnetosphere: A Cluster study, *Ann. Geophys.*, *23*, 2679–2686.

Etcheto, J., P. J. Christiansen, M. P. Gough, and J. G. Trotignon (1982), Terrestrial continuum radiation observations with GEOS-1 and ISEE-1, *Geophys. Res. Lett.*, *9*, 1239–1242, doi:10.1029/GL009i011p01239.

Gough, M. P. (1982), Non-thermal Continuum emissions associated with electron injections: Remote plasmapause sounding, *Planet. Space Sci.*, *30*, 657–668, doi:10.1016/0032-0633(82)90026-5.

Gough, M. P., P. J. Christiansen, G. Martelli, and E. J. Gershuny (1979), Interaction of electrostatic waves with warm electrons at the geomagnetic equator, *Nature*, *279*, 515–517, doi:10.1038/279515a0.

Gurnett, D. A. (1975), The Earth as a radio source: The nonthermal continuum, *J. Geophys. Res.*, *80*, 2751–2763, doi:10.1029/JA080i019p02751.

Gurnett, D. A., and L. A. Frank (1976), Continuum radiation associated with low-energy electrons in the outer radiation zone, *J. Geophys. Res.*, *81*, 3875–3885, doi:10.1029/JA081i022p03875.

Gustafsson, G., et al. (1997), The electric field and wave experiment for the Cluster mission, *Space Sci. Rev.*, *79*, 137–156, doi:10.1023/A:1004975108657.

Hudson, M., R. Denton, M. Lessard, E. Miftakhova, and R. Anderson (2004), A study of Pc-5 ULF oscillations, *Ann. Geophys.*, *22*, 289–302.

Hughes, W. J., R. L. McPherron, and C. T. Russell (1977), Multiple satellite observations of pulsation resonance structure in the magnetosphere, *J. Geophys. Res.*, *82*(4), 492–498, doi:10.1029/JA082i004p00492.

Kasaba, Y., H. Matsumoto, K. Hashimoto, R. R. Anderson, J. L. Bougeret, M. L. Kaiser, X. Y. Wu, and I. Nagano (1998), Remote sensing of the plasmapause during substorms: Geotail observation of nonthermal continuum enhancement, *J. Geophys. Res.*, *103*, 20,389–20,405, doi:10.1029/98JA00809.

Kennel, C. F., et al. (1970), VLF electric field observations in the magnetosphere, *J. Geophys. Res.*, *75*, 6136–6152, doi:10.1029/JA075i031p06136.

Kurth, W. S. (1992), Continuum radiation in planetary magnetospheres, in *Planetary Radio Emission III*, edited by H. O. Rucker, S. J. Bauer, and M. L. Kaiser, pp. 329–350, Austrian Acad. of Sci., Vienna.

Kurth, W. S., D. A. Gurnett, and R. R. Anderson (1981), Escaping nonthermal continuum radiation, *J. Geophys. Res.*, *86*, 5519–5531, doi:10.1029/JA086iA07p05519.

Loewe, C. A., and G. W. Prölss (1997), Classification and mean behavior of magnetic storms, *J. Geophys. Res.*, *102*(A7), 14,209–14,213, doi:10.1029/96JA04020.

Loto'Aniu, T. M., B. J. Fraser, and C. L. Waters (2009), The modulation of electromagnetic ion cyclotron waves by Pc 5 ULF waves, *Ann. Geophys.*, *27*(1), 121–130.

Mager, P. N., and D. Y. Klimushkin (2006), On impulse excitation of the global poloidal modes in the magnetosphere, *Ann. Geophys.*, *24*, 2429–2433.

Mann, I. R., and A. N. Wright (1995), Finite lifetimes of ideal poloidal Alfvén waves, *J. Geophys. Res.*, *100*(A12), 23,677–23,686.

Melrose, D. B. (1981), A theory of non-thermal continua in the terrestrial and jovian magnetospheres, *J. Geophys. Res.*, *86*, 30–36, doi:10.1029/JA086iA01p00030.

Morgan, D. D., and D. A. Gurnett (1991), The source location and beaming of terrestrial continuum radiation, *J. Geophys. Res.*, *96*, 9595–9613, doi:10.1029/91JA00314.

Oya, H. (1971), Conversion of electrostatic plasma wave into electromagnetic waves: Numerical calculation of the dispersion relation for all wavelengths, *Radio Sci.*, *6*, 1131–1141, doi:10.1029/RS006i012p01131.

Pierrard, V., and J. F. Lemaire (2004), Development of shoulders and plumes in the frame of the interchange instability mechanism for plasmapause formation, *Geophys. Res. Lett.*, *31*, L05809, doi:10.1029/2003GL018919.

Rönnmark, K. (1985), Generation of magnetospheric radiation by decay of Bernstein waves, *Geophys. Res. Lett.*, *12*, 639–642, doi:10.1029/GL012i010p00639.

Schäfer, S., K. H. Glassmeier, P. T. I. Eriksson, P. N. Mager, V. Pierrard, K. H. Fornaçon, and L. G. Blomberg (2008), Spatio-temporal structure of poloidal Alfvén wave detected by Cluster adjacent to the dayside plasmapause, *Ann. Geophys.*, *26*, 1805–1817.

Singer, H. J., W. J. Hughes, and C. T. Russel (1982), Standing hydromagnetic waves observed by ISEE1 and 2: Radial extend and harmonic, *J. Geophys. Res.*, *87*, 3519–3529, doi:10.1029/JA087iA05p03519.

Takahashi, K., and B. J. Anderson (1992), Distribution of ULF energy (f is less than 80 mHz) in the inner magnetosphere: A statistical analysis of AMPTE CCE magnetic field data, *J. Geophys. Res.*, *97*, 10,751–10,773, doi:10.1029/92JA00328.

Tsyganenko, N. A. (1989), A Magnetospheric magnetic field model with a warped tail current sheet, *Planet. Space Sci.*, *37*, 5–20, doi:10.1016/0032-0633(89)90066-4.

P. M. E. Décréau, G. Le Rouzic, X. Suraud, and X. Vallières, Laboratoire de Physique et Chimie de l'Environnement et de l'Espace, CNRS, 3A Ave. de la Recherche Scientifique, F-45071 Orléans CEDEX 2, France.

C. Foullon, Centre for Fusion, Space and Astrophysics, Department of Physics, University of Warwick, Coventry CV4 7AL, UK.

S. Grimald, Mullard Space Science Laboratory, University College London, Surrey RH5 6NT, UK. (sg2@mssl.ucl.ac.uk)